International Journal of Engineering Trends and Technology
ISSN: 2231-5381/ https://doi.org/10.14445/22315381/IJETT-V73I3P131

Volume 73 Issue 3, 448-460, March 2025

Original Article

A Novel Tropical Cyclone Intensity Prediction with Cyclone Classification Using Improved Dung Beetle Optimization with Deep Learning

S. Jayasree[1*], K. R. Ananthapadmanaban[1]

[1]*Department of Computer Science, SRM Institute of Science and Technology, Vadapalani Campus, Chennai, India.*

[*]*Corresponding Author : subrad1997@gmail.com*

Received: 18 July 2024 Revised: 06 February 2025 Accepted: 25 February 2025 Published: 28 March 2025

Abstract - *Tropical Cyclones (TCs) contribute crucially to financial damage and loss of lives in coastal regions. As a result, TC prediction becomes a crucial research area. Estimating the intensity of TCs is beneficial for reducing and preventing the effects of natural disasters. Lately, intensity prediction remains a challenge, and TC track prediction has progressed considerably due to the complicated system of TC. Accurately estimating the TC intensity is vital for disaster management in the meteorological industry and initialization in prediction models. It is also crucial to forecasting and understanding the behaviour of TC. Moreover, cyclone classification consists of classifying cyclones according to their intensity, structure, and other meteorological features. Typically, this technique uses different criteria: organization of cloud patterns, wind speed, and central pressure. At present, the fast evolution of Deep Learning (DL) has resulted in an abundance of research using it in TC grading and TC intensity estimation. This manuscript presents a novel TC Intensity Prediction with Cyclone Classification using an Improved Dung Beetle Optimization with DL (TCIPCC-IDBODL) approach. The TCIPCC-IDBODL approach aims to predict the TC intensity and classify TC into various types. The TCIPCC-IDBODL technique follows a series of operations to estimate TC intensity and classify TC types, such as pre-processing, feature extraction, and classification. Initially, the TCIPCC-IDBODL technique pre-processes the input images via Wiener Filtering (WF)-based noise elimination and Dynamic Histogram Equalization (DHE)-based contrast enhancement. In the TCIPCC-IDBODL technique, the Squeeze-Excitation EfficientNet (SE-EfficientNet) model derives feature vectors from the pre-processed images. Moreover, the Stacked Sparse AutoEncoder (SSAE) model is used for prediction and classification. Furthermore, the hyperparameter tuning of the SSAE network is accomplished by employing the IDBO method. A range of investigations was involved in portraying the more significant achievement of the TCIPCC-IDBODL method. The performance validation of the TCIPCC-IDBODL method demonstrated a superior accuracy value of 95.12% over existing models.*

Keywords - *Tropical Cyclones (TCs), Weather prediction, Dung beetle optimization, Deep Learning (DL), Dynamic Histogram Equalization (DHE).*

1. Introduction

The TCs are extreme weather conditions that may severely threaten human life [1]. The heavy rainfall and strong winds accompanying this system can hamper social and economic development in the affected region and cause substantial property damage. As a result, accurately estimating the TC intensity is needed for both practical and theoretical research applications [2]. The most popular approach, the Dvorak, is employed to assess the intensity of TC, which correlates the shape of the eye, rotation, and thunderstorm activity of TC with its weakening or strengthening [3]. This procedure needs expert evaluation of infrared and visible satellite imaging of the TC's cloud patterns and assumes that cyclones with the same intensities frequently have the same patterns [4]. Further, the method analyzes rainfall rates, curvature radius, core features, and cloud organization characteristics to estimate the storm intensity once the relevant patterns are detected. It is highly subjective since this technique heavily relies on professional experience [5]. Based on past information and expert evaluation, classical meteorological methods often encounter difficulties in accurately representing unpredictable and quick variations in TC intensity, producing more inaccurate predictions that may threaten public safety [6]. Although advanced resolution and parameterization problems are encountered, Numerical Weather Prediction (NWP) models have been constrained to replicate the development of cyclones. Even though Ensemble Prediction Systems (EPS) give probabilistic details, they may not be entirely responsible for all the uncertainty causes and can be computationally expensive [7]. Incorporating new

scientific concepts into anticipating practices can be hindered by a few classical techniques dependent on heuristic criteria and empirical relationships. Data-based models have gained popularity in recent years, significantly improving predictive accuracy and performance in complex applications [8]. Convolutional Neural Networks (CNN) include fully connected and convolutional layers, where the former extracts spatial characteristics from the input image and has a simple computational unit. CNN is used for extraction, similar to how weather forecasters recognize cloud structures (viz., hurricane eyes) related to TCs within the specific intensity range. This feature is used as a predictor for estimating the intensity of TC [9]. Some research workers have implemented CNN to classify TC intensity. TCs are major threats to life and property, making accurate intensity prediction vital. Conventional methods such as Dvorak have limitations in complex data handling. This emphasizes the requirement for advanced DL and optimization techniques to improve prediction accuracy [10].

This manuscript presents a novel TC Intensity Prediction with Cyclone Classification using an Improved Dung Beetle Optimization with DL (TCIPCC-IDBODL) approach. The TCIPCC-IDBODL approach aims to predict the TC intensity and classify TC into various types. The TCIPCC-IDBODL technique follows a series of operations to estimate TC intensity and classify TC types, such as pre-processing, feature extraction, and classification. Initially, the TCIPCC-IDBODL technique pre-processes the input images via Wiener Filtering (WF)-based noise elimination and Dynamic Histogram Equalization (DHE)-based contrast enhancement. In the TCIPCC-IDBODL technique, the Squeeze-Excitation EfficientNet (SE-EfficientNet) model derives feature vectors from the pre-processed images. Moreover, the Stacked Sparse Autoencoder (SSAE) model is used for prediction and classification. Furthermore, the hyperparameter tuning of the SSAE network is accomplished by employing the IDBO method. A range of investigations was involved in portraying the more significant achievement of the TCIPCC-IDBODL method.

The key contribution of the TCIPCC-IDBODL method is listed below.

- WF effectively eliminates noise from the input data, improving the overall quality. This step significantly improves the signal clarity, improving performance in subsequent processing stages.
- The DHE model improves the contrast of the images, enhancing the visibility of key features. This technique assists in better distinguishing significant details for more accurate analysis and classification.
- The SE-EfficientNet method is implemented to extract effective feature vectors, employing an advanced DL technique. This methodology improves feature extraction and enables better representation of complex patterns in the data.
- The SSAE technique is utilized for accurate intensity prediction and classification, enhancing the capability of the model to capture crucial features. This technique improves overall performance by refining input data representation for better predictive accuracy.
- IDBO is a novel optimization technique for fine-tuning the model. It improves the effectiveness and accuracy of the feature extraction and prediction process. The key innovation is its capability to optimize complex models by balancing exploration and exploitation, improving overall performance.

2. Related Works

In [11], a system dependent upon adaptive weight learning networking (AWL-Net) was developed. Furthermore, a multi-branch model was built, and AWL was devised. The 3D Conv. Gated Recurrent Unit (3D ConvGRU) is employed based on the 3D dynamic features of TCs for accomplishing feature improvement, followed by 3DCNN, which should be implemented for capturing and learning TC temporal and spatial features. Tan et al. [12] introduced an objective DL-based technique.

The fundamental architecture of the model is a CNN method. Likewise, attention mechanisms and residual learning have been embedded into the system. 5 cloud products with level 2 items at the geostationary satellite H-8 must be implemented as the inputs of model training. In [13], a dynamic balance CNN method was presented. It encompasses two branches.

In conclusion, the architecture is rapidly modified by adaptable tradeoff parameters, progressively in the learning raw data for learning strong TCs, hence lessening the errors. Also, an attention mechanism was utilized to acquire connections among channels to increase additional TC intensity. Tian et al. [14] introduced a spatiotemporal attention Convolutional Network (STACPred) model, which utilizes DL methods to allow real-time forecast of TC intensity and develop the spatiotemporal features of TCs.

This method utilizes dual branches for the extraction and integration of features. Moreover, a Residual Attention (RA) method was incorporated. Furthermore, a Rolling Mechanism (RM) was utilized. In [15], a DL-based method called TC-Resnet, integrating infrared and microwave satellite information, was developed. This study considered the resnet50 architecture as the fundamental architecture and embedded a convolution layer with 5×5 convolutional kernels.

Also, the integrated channel spatial dual attention module is presented. Vahidhabanu et al. [16] developed a DL-CNN model. A CNN-based technique has been employed to recognize cyclone constituents. The CNN technique has been used, whereas AlexNet could extract the features, construct the architecture, and predict cyclone environments. Moreover,

the Convolutional Block Attention Module (CBAM) method, dependent upon 3D, has been employed to demonstrate visual attention for increasing the model's vital channels and primary cloud model. Wang et al. [17] introduced a DL method for predicting TC intensity in the Northwest Pacific. The w-, v- and u-elements of IR satellite images, wind, ocean surface temperature, and previous TC data have been chosen as input. Subsequently, the TC Intensity Forecasting fusion (TCIF-fusion) method was presented. In conclusion, heatmaps capturing system insights could be produced and implemented into the original input data. In [18], DL integrated infrared with microwave satellite images. The main idea could be developed.

The residual images among features of past satellite image sequences and existing satellite images were captured as the last feature matrix. Multilayer ConvLSTM has been utilized for feature extraction. Zhang et al. [19] propose a double-layer encoder-decoder model for TC intensity estimation. The model includes wavelet transform for high-frequency extraction, multi-channel image fusion, and TC intensity estimation.

Yang et al. [20] improve TC intensity estimation by utilizing pre-trained CNNs on geostationary satellite infrared imagery, with improvements like fine-tuning, augmentation, and physical data integration, ultimately optimizing a VGGNet model. Tong et al. [21] utilize DL to model TCG patterns using Variational Autoencoder (VAE) for direct simulation and CNN to explore environmental effects. Ham et al. [22] developed the DeepTC CNN methodology, utilizing a unique amplitude focal loss for capturing rapid intensification events.

Lv et al. [23] present an LSTM model to predict typhoon maximum wind speeds utilizing atmospheric forecasts, constructing a parametric wind field methodology and optimizing it with numerical method wind fields. Krishna et al. [24] utilize DL with satellite and grayscale images to enhance cyclone intensity prediction. CNNs extract patterns from both image modalities, integrating them through a novel architecture for more accurate intensity estimation. Wang et al. [25] improve long-term TC intensity forecasting by improving TC intensity-spatial information matching and integrating physical knowledge, utilizing the VQLTI framework.

Mawatwal and Das [26] present a hybrid model using a CNN for cyclone intensity prediction based on IR satellite imagery. It incorporates a binary and multiclass classifier, regression module, and YOLOv3 cyclone detector to improve prediction accuracy.Despite significant advancements in DL-based TC intensity prediction, various limitations remain. Many existing models face difficulty with long-term forecasting accuracy and handling the complex dynamics of TCs.

Furthermore, the reliance on limited or incomplete data, such as satellite imagery alone, may mitigate model generalization. Moreover, incorporating physical constraints and spatiotemporal features remains a challenge for improving prediction precision. A gap exists in developing robust models that can effectively integrate real-time data and physical knowledge to enhance forecasting accuracy over extended periods.

3. The Proposed Method

This paper presents the TCIPCC-IDBODL approach, which aims to predict the TC intensity and classify TC into various types. The TCIPCC-IDBODL technique follows a series of operations to estimate TC intensity and classify TC types. Figure 1 demonstrates the architecture of the TCIPCC-IDBODL method.

3.1. Pre-Processing

Initially, the TCIPCC-IDBODL technique pre-processes the input images via WF-based noise removal and DHE-based contrast enhancement [27]. Using WF and DHE for contrast enhancement presents significant advantages in improving image quality for analysis. WF mitigates noise without blurring crucial features, ensuring more apparent input data. DHE enhances image contrast, making subtle details more visible, which is significant for accurate feature extraction.

These techniques were chosen over others due to their capability to preserve critical data while improving image clarity, thus improving the overall performance of subsequent models.WF is a robust mechanism for eliminating noise in image processing involving RS applications.

Unlike classical linear filters, WF considers the statistical properties and noisy images. By modelling the desired signal and the noise spectrum, WF aims to diminish MSE and efficiently overwhelm noise while maintaining image detail and sharpness. In RSI, images frequently suffer from various noise sources like atmospheric interference and sensor artefacts; WF presents a promising solution for improving subsequent analysis tasks' accuracy and enhancing image quality.

DHE is a versatile technique for contrast enhancement in RSI [28]. DHE operates locally, changing the contrast based on the features of the image region, which is different from classical histogram equalization, which redistributes pixel intensity globally over the entire image. This enables the enhancement of bright and dark areas, enhancing the image's visual quality and successfully bringing out fine details. In the RSI application, images often display varying terrain conditions and uneven illumination. DHE achieved outstanding results in improving interpretability and facilitating accurate analysis, such as feature detection and classification.

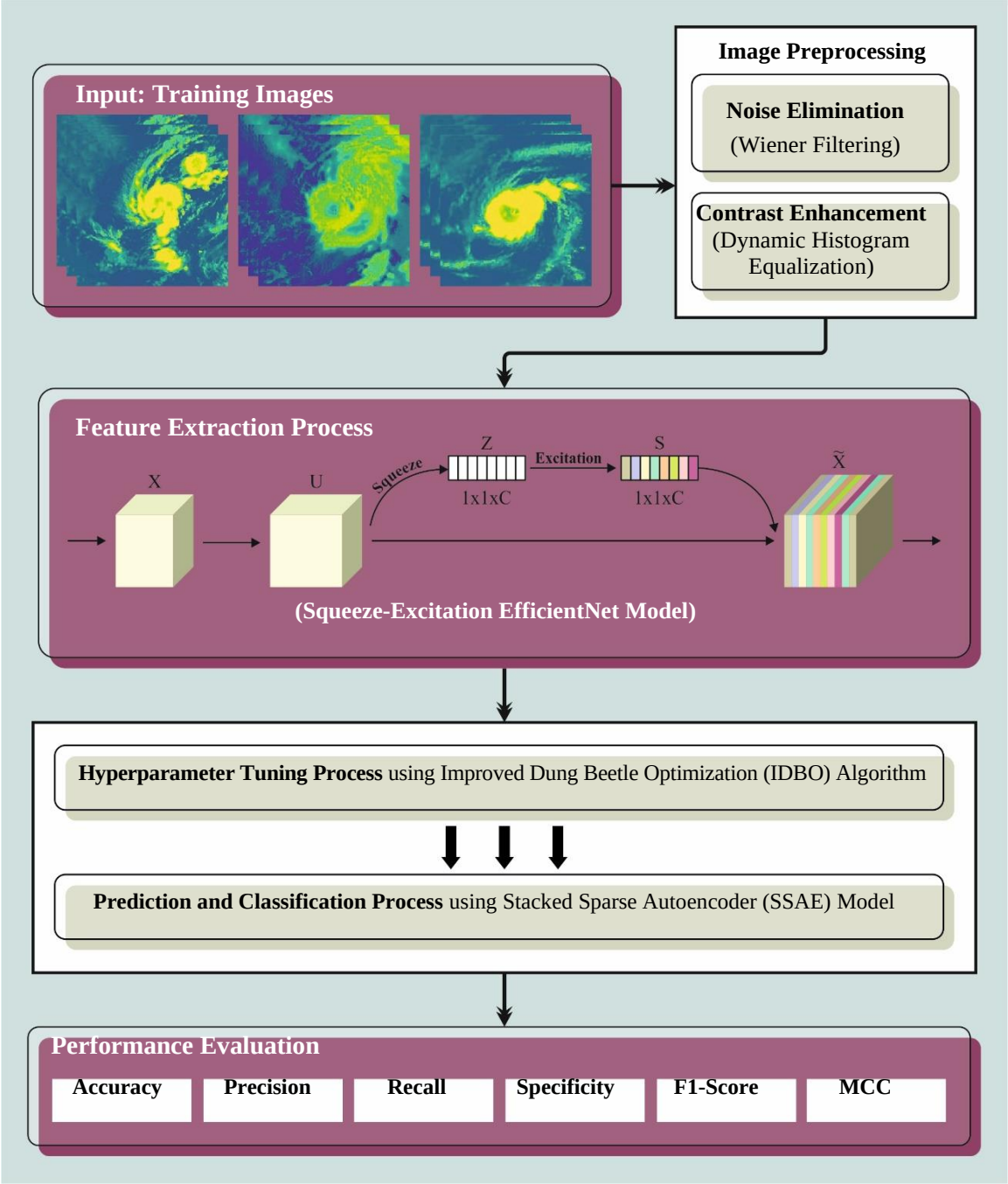

Fig. 1 Architecture of TCIPCC-IDBODL technique

3.2. SE-EfficientNet Model

This technique is utilized for the feature extraction process to derive feature vectors from the pre-processed images [29]. This model was chosen due to its efficient architecture, which balances high performance with low computational cost. The SE mechanism improves the capability of the model to capture crucial features by focusing on channel-wise dependencies, improving feature representation. EfficientNet's scaling method allows it to adapt to diverse image sizes without excessive resource usage, making it more efficient than conventional CNN architectures. This combination of efficiency and accuracy makes SE-EfficientNet ideal for extracting meaningful features from complex datasets.

The achievement has improved, so the methods utilized in the dataset of ImageNet have turned into more compound, but numerous models are not efficient when using load calculating. The EfficientNet method, between the advanced techniques, attained an accuracy of 84.4 percent with 66 *M*

parameters in the ImageNet identification issue that can be reflected as a set of CNN methods. EfficientNet set has eight techniques among B0 and B7, and if the method quantity rises, the intended parameters will not upsurge greatly, but accuracy rises prominently. When equated to CNN approaches, EfficientNet utilizes an innovative activation function called Swish rather than the ReLU.

The DL aims to show additional effective methodologies with lesser methods. EfficientNet attains more effectual outcomes by evenly scaling width, depth, and resolution while ascending down the technique. The 1st stage in the complex scaling model is to explore a system to determine the relation among the dissimilar scale dimensions of the base model below the resource limitation.

This technique defined an appropriate scaling factor for width, resolution and depth dimensions. Next, the co-efficient extended the base method to the preferred target system. The primary structure block of EfficientNet is the reversed bottleneck, originally introduced in MobileNetV2. However, it is used more efficiently in EfficientNet due to its higher floating-point operations per second (FLOPS). This block contains a layer that first enlarges and then compacts the network. Therefore, straight networks were employed among bottlenecks, which attach fewer networks than the expansion layer. This structure has in-depth separate convolutional decrease computation by nearly k^2 factor when equated to the classical layer. However, k denotes the kernel size of the $2D$ convolution model.

In complex scaling, the co-efficient ϕ was utilized with the value assumed in Equation (1) to compute width, resolution and depth evenly.

$$\begin{gathered} depth: d = \alpha^{\psi} \\ width: w = \beta^{\psi} \\ resolution: r = \gamma^{\psi} \\ \alpha \geq 1, \beta \geq 1, \gamma \geq 1 \end{gathered} \tag{1}$$

Here, α,β,γ denotes the coefficients chosen by network search. ϕ represents the user-defined coefficient, which manages the sources obtainable for scaling, where γ, β, α define how additional resources were consigned to the resolution, depth and width correspondingly.

In a steady convolutional method, FLOPS have been relative to d, w^2, r^2. Then, the cost of calculating in the convolution network is high owing to convolutional processes, scaling the convolutional network as set in Eq. (1) upsurges the FLOPS of the method by nearly $(\alpha, \beta^2, \gamma^2)^{\phi}$ $(\alpha . \beta^2 y^2)^{\phi}$ in total.

Beginning from B0, the complex scaling model measures this approach in dual steps:

Step1: Let's assume dual resources are available, grid exploration is implemented with $\phi = 1$, and the finest values were created for α, β, γ.

Step2: Achieved α, β, γ values were chosen as constant, and the network of the base has been measured to acquire EffcientNetB1 to B7 applying Eq. (1) with diverse ϕ values.

The SE block implements feature recalibration for transformation. F_{tr} mapping the input X to the feature map U, in which $U \in \mathcal{R}^{H \times W \times C}$, viz., a convolution, [30]. A squeeze function is performed by the features U is passed first, and later, a channel descriptor is produced by integrating the feature map through the spatial dimension $H \times W$.

This mainly produces an embedding of the global dispersion of channel-wise feature response, allowing each layer to utilize the data from the global receptive field. Then, a self-gating model where a channel modulation weight is generated by considering the embedding as the given input. This is known as the excitation function. The weight produces the SE block's output through the feature map and is loaded into succeeding layers.

3.3. SSAE-Based Classification Process

At this stage, the SSAE model is used for prediction and classification [31]. This model was chosen because it can effectively learn hierarchical features from high-dimensional data. SSAE outperforms extracting meaningful patterns by enforcing sparsity, resulting in improved generalization and mitigated overfitting.

This model is specifically effective in handling complex and noisy data, as it learns an optimal representation through multiple layers of encoding. SSAE presents superior feature learning and classification performance compared to other techniques, particularly in cases with limited labelled data. Figure 2 portrays the infrastructure of SSAE.

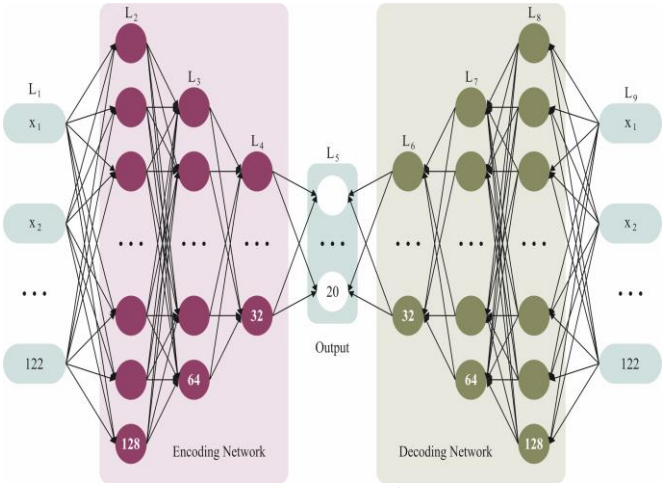

Fig. 2 Architecture of SSAE

An AE is an unsupervised learning method that mechanically acquires the feature of raw data and contains three layers: the input, output, and hidden layer (HL). The encoder system has an input and HL, and the decoder network has an output and HL. The encoder network removes the feature from the unique data, where the decoder rebuilds the input data over the feature. $X = [X_1, X_2, \cdots, X_n]^T$ denotes input and n refers to the nodes in the input layer, demonstrating the sample data size. The HL (h) of the novel data X acquired over the encoding network was intended below:

$$h = f(WX + b) \tag{2}$$

Here, h denotes the feature parameter removed by the encoder; f represents the activation function, where Sigmoid is commonly nominated; b and W refer to biases and weights utilized in the encoder stage, correspondingly; and the size of W is $s \times n$, whereas s indicates the size of the feature parameter. The decoder system was employed to rebuild the unique input data, and then recreated data Y is attained after decoder the HL feature h, as below:

$$Y = U(W'h + b') \tag{3}$$

Wherein $Y = [Y_1, Y_2, \cdots, Y_n]^T$ specifies the output of network data; U denotes the Sigmoid activation function in the decoder method; W' and b' refer to the weight and bias applied in the encoder stage, correspondingly; and $W' = W^T$. The AE employs Stochastic Gradient Descent (SGD) and backpropagation (BP) models to enhance the set of parameters $\theta = \{W, b, W', b'\}$ to diminish faults among, output and input data. Generally, the function of the Mean Square Error (MSE) was determined as loss function is given below:

$$J_{MSE}(\theta) = \frac{1}{m}\sum_{i=1}^{m}\frac{1}{2}\|X^{(i)} - Y^{(i)}\|^2 \tag{4}$$

Here, m denotes the overall training samples; $Y^{(i)}$ and $X^{(i)}$ specify the output and original data of the ith sample, correspondingly. The SAE is built by inserting a word of sparse penalty to the cost function of AE. It generally absorbs more abstract and typical density features, which are highly latent. The term sparse penalty was determined below:

$$J_{spare}(\theta) = \beta \sum_{j=1}^{s} K\, L(\rho \| \hat{\rho}_j) \tag{5}$$

$$KL(\rho \| \hat{\rho}_j) = \rho \log_2 \frac{\rho}{\hat{\rho}_j} + (1-\rho)\log\frac{1-\rho}{1-\hat{\rho}_j} \tag{6}$$

$$\hat{\rho}_j = \frac{1}{m}\sum_{i=1}^{m}(a_j X^{(i)}) \tag{7}$$

In Equation (5), β portrays the factor of sparse penalty, employed to handle the weight in the function of loss; ρ is the sparse parameter; s refers to the size of HL; $\hat{\rho}_j$ represents the average activation value. Equation (6) represents the relative entropy computation formulation applied to extend the deviation grade among dual distributions. Equation (7) computes the value of average activation, whereas a_j specifies the quantity of action in $a\ jth$ unit of HL. Equation (8) is the SAE loss function. The 1st term denotes the MSE function, and the 2nd is the sparse penalty.

$$J(\theta) = J_{MSE}(\theta) + J_{sparse}(\theta) \tag{8}$$

An SSAE is a DNN technique collected of manifold SAEs. By compelling the HL of the preceding SAE as an input of the subsequent SAE, every HL is a nonlinear map depicting the preceding layer output. With every further HL, the system can compute complex nonlinear map relations. It will get the inventive data's highest and lowest dimension features, so this technique contains expression capability and robust feature extraction.

3.4. Hyperparameter Tuning Utilizing IDBO

Lastly, the SSAE network tuning is achieved using the IDBO technique [32]. This method is highly effective because it can balance exploration and exploitation in the search space. IDBO is appropriate for complex optimization tasks as it effectively navigates large and multi-dimensional parameter spaces, avoiding local minima. Unlike conventional optimization methods, IDBO adapts dynamically to the problem, enhancing accuracy and convergence speed. Its robustness in handling various model parameters makes it a superior choice for fine-tuning models and improving performance over other optimization techniques. Figure 3 depicts the steps involved in the IDBO model.

Fig. 3 Steps involved in the IDBO method

DBO is a novel population intellect optimizer algorithm stimulated by the Dung Beetles' (DB) performances, such as searching, dancing, breeding, ball rolling, and theft. This model has been considered for its higher accuracy and speed of convergence. The DBO method attains a parameter optimizer by executing equivalent processes with DBs of dissimilar behaviour kinds. It was precisely separated into four tactics.

Tactic 1: Ball Rolling

DBs generally utilize the sun as a monitor to ensure that they roll the balls directly, but standard features like wind and light force will disturb ball rolling at the time of migration. The DB's position while the ball rolling was upgraded depended upon Equations (9) and (10).

$$x_i^{t+1} = x_i^t + \alpha \times k \times x_i^{t-1} + b \times \Delta x \quad (9)$$

$$\Delta x = |x_i^t - X^w| \quad (10)$$

Whereas x_i^t represents the 1st iteration of t position data of the ith DB; $k \in (0.0,0.2)$ represents the co-efficient of defection; X^w indicates the location of global worst; t signifies the present iteration count; Δx is utilized to pretend variations in light power; α denotes the average coefficient representing if it has differed from its original way and allocated as -1 or 1, $b \in (0.0,1.0)$ signifies a stable parameter. If a DB meets a complication, it prohibits its rolling track, so it wants to relocate itself by dancing to discover a novel rolling way. To pretend this, a tangent function is employed to get the novel rolling. The DBs will roll the ball once the novel rolling way is defined. The novel location has been upgraded as per Equation (11).

$$x_i^{t+1} = x_i^t + \tan\theta |x_i^t - x_i^{t-1}| \quad (11)$$

Here, if θ is equivalent to 0, $\frac{\pi}{2}$, or π, $\theta \in [0, \pi]$ signifies the direction of defection. The DB location has not been upgraded.

Tactic 2: DBs with Ovoid Ball (Rood Ball)

Naturally, DBs roll the ball to a secure location to cover it so that female beetles can lay the eggs in an appropriate situation. The laying region was demonstrated and subsequent in Equations (12) and (13).

$$Lb^* = \max(X^* \times (1 - R), Lb) \quad (12)$$

$$Ub^* = \min(X^* \times (1 + R), Ub) \quad (13)$$

Here, X^* denotes the existing local optimal location, $and\ Lb^*$ and Ub^* specify the lower and upper boundaries of the laying area. Initial weights $R = 1 - \frac{t}{T_{\max}}$. Ub and Lb epitomize the limitations of the optimizer issue. $T_{\max}$ signifies the highest iteration count; the modification of spawn balls is definite in Equation (14).

$$B_i^{t+1} = X^* + b_1 \times (B_i^t - Lb^*) + b_2 \times (B_i^t - Ub^*) \quad (14)$$

Whereas B_i^t refers to the tth iteration of i; b_1 and b_2 denote the unrelated randomly produced vectors that demonstrate the number of sizes.

Tactic 3: Foraging of Young DBs

The eggs placed by female DBs slowly mature into baby DBs, and a few of the matured babies hunt for food in the optimum searching region definite by Equations (15) and (16).

$$Lb^b = \max(X^b \times (1 - R), Lb) \quad (15)$$

$$Ub^b = \min(X^b \times (1 + R), Ub) \quad (16)$$

Here, Ub^b and Lb^b represent the upper and lower bounds correspondingly; b denotes the location of a global optimum. The place upgrade is a result of Equation (17).

$$x_i^{t+1} = x_i^t + C_1 \times (x_i^t - Lb^b) + C_2 \times (x_i^t - Ub^b) \quad (17)$$

Whereas, x_i^t denotes the tth iteration of i; C_1 refers to the randomly produced value which tracks a normal distribution; $C_2 \in (0.0,1.0)$, which has been randomly generated vector.

Tactic 4: The Behaviour of Stealing (Thief)

Few DBs are recognized as stealing DBs, taking others' food and egg balls. Equation (18) simplified the location of this behaviour.

$$x_i^{t+1} = X^b + S \times g \times (|x_i^t = X^*| + |x_i^t - X^b|) \quad (18)$$

Here, S indicates a constant value; g indicates the randomly generated vector size of $1 \times D$ by following a normal dispersion; and X^b denotes the optimum food source. The improved DBO method integrates Oppositional-Based Learning (OBL) with the conventional DBO method. OBL is a robust optimization enhancement method in intellect computation [33]. Typically, metaheuristic algorithms commence with a random initial solution and frequently attempt to dislocate nearer to the finest global solution. The search procedure arises when exact pre-determined desires are met. Due to the lack of valid advanced data, convergence needs significant time. OBL integrates a new tactic to find out this, simultaneously evaluating the existing solution's fitness value and the similar opposite solution.

Then, the better individual is kept for the subsequent iteration, supporting population change efficiently. Specifically, the opposition candidate solution consists of a fifty percent greater opportunity of being nearer to the global optimal when equated to other existing solutions. Therefore, OBL has attained extensive support as it suggestively improves the optimizer performance of numerous metaheuristic algorithms. The OBL mathematical calculation is as follows:

$$\hat{X} = lb + ub - X. \quad (19)$$

Here, $\hat{X}$ denotes the opposing solution, and X signifies the existing solution. ub and lb are the upper and lower limits, subsequently. OBL has the restraint of generating the

opposing solution at an assumed location. This technique is shown during the primary optimizer stages. However, when the search evolves, there is a prospect that the opposing solution may close up near a local optimal. Therefore, other individuals may drop near this region quickly, resulting in early conjunction and decreased accuracy. In this problem, the Random OBL (ROBL) tactic includes random perturbation to adjust Equation (19). Fitness selection is a crucial factor that influences the success of the IDBO model. The hyperparameter selection process comprises encoding the solution to evaluate candidate solutions. In the IDBO model, accuracy is now considered the significant factor in designing the FF.

$$Fitness = \max(P) \tag{20}$$

$$P = \frac{TP}{TP+FP} \tag{21}$$

Here, TP and FP depict true and false positive values.

4. Performance Validation

The investigational assessment of the TCIPCC-IDBODL method is conducted using INSAT3D Infrared and Raw Cyclone Imagery from the Kaggle repository [34]. This dataset includes all INSAT3D-captured imageries over the Indian Ocean from 2012 to 2021, along with cyclone intensity in knots. Figures 4 and 5 demonstrate the sample TC raw and inferred images.

Since this work focuses on the classification of TCs, it can be divided into four types based on their intensity, as shown in Figure 6 and listed below.

- Class 1-Typhoon (TY, 35–63 kt)
- Class 2-Strong Typhoon (STY, 64-84 kt),
- Class 3-Very Strong Typhoon (VSTY, 85-104 kt)
  Class 4-Violent Typhoon (VTY, >105 kt).

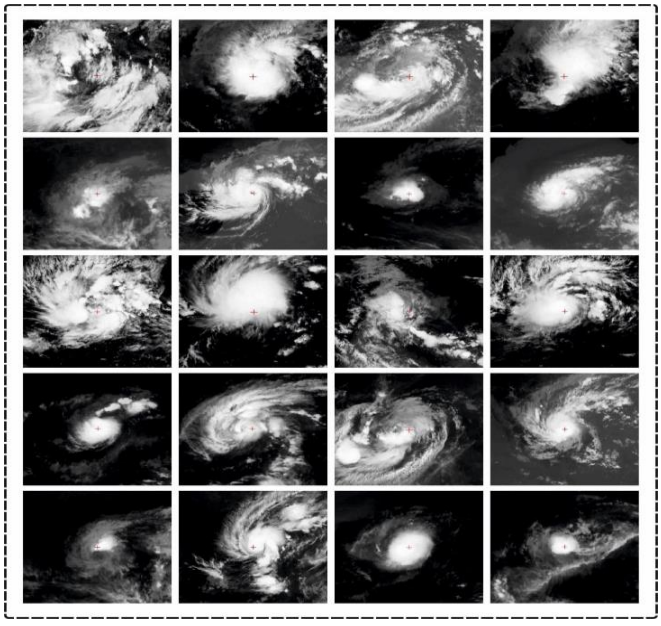

Fig. 4 Sample Images TC (Raw Images)

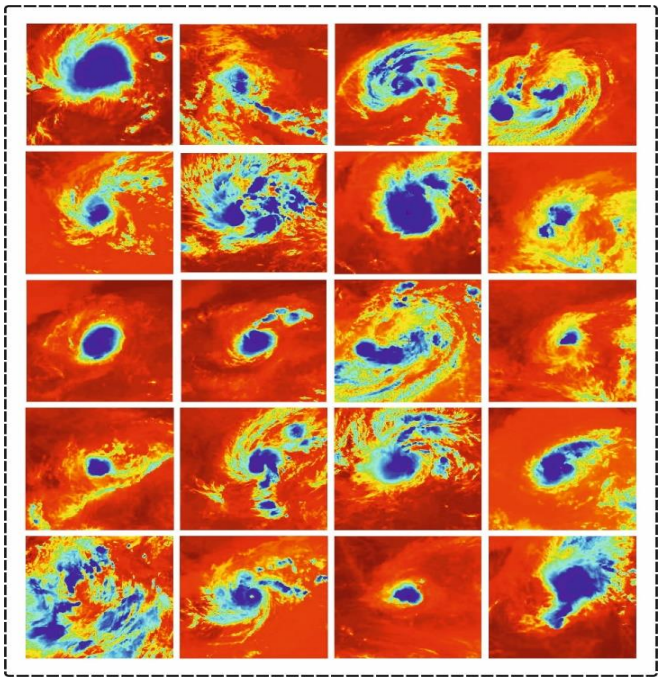

Fig. 5 Sample Images TC (Infrared Images)

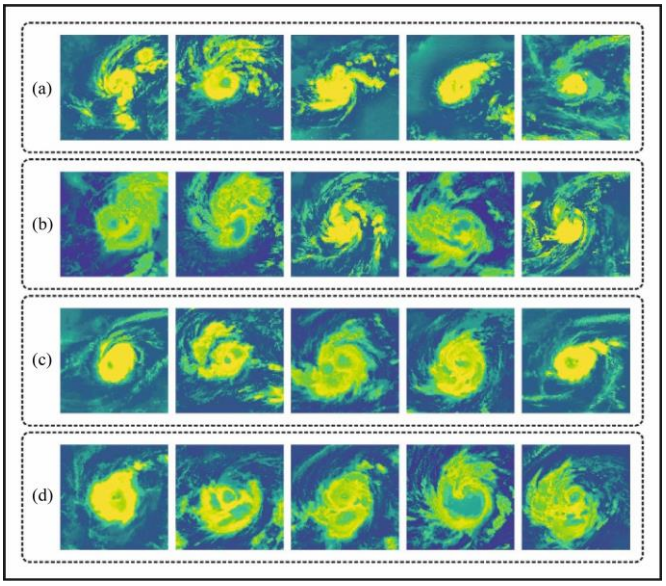

Fig. 6 Extracted Features a) Typhoon b) Strong Typhoon c) Very Strong Typhoon d) Violent Typhoon

The performance of the TCIPCC-IDBODL method on the training set is demonstrated in Figure 7. The confusion matrix illustrated by the TCIPCC-IDBODL method is described in Figure 7a. The simulation value denoted that the TCIPCC-IDBODL model has precisely detected and classified the overall four classes. Likewise, the PR investigation of the TCIPCC-IDBODL model is shown in Figure 7b. The results illustrated that the TCIPCC-IDBODL technique has attained higher PR values on each class label. Lastly, the ROC examination of the TCIPCC-IDBODL method is depicted in Figure 7c. The experimental value illustrated that the

TCIPCC-IDBODL method has given an outcome with higher ROC on distinct classes.

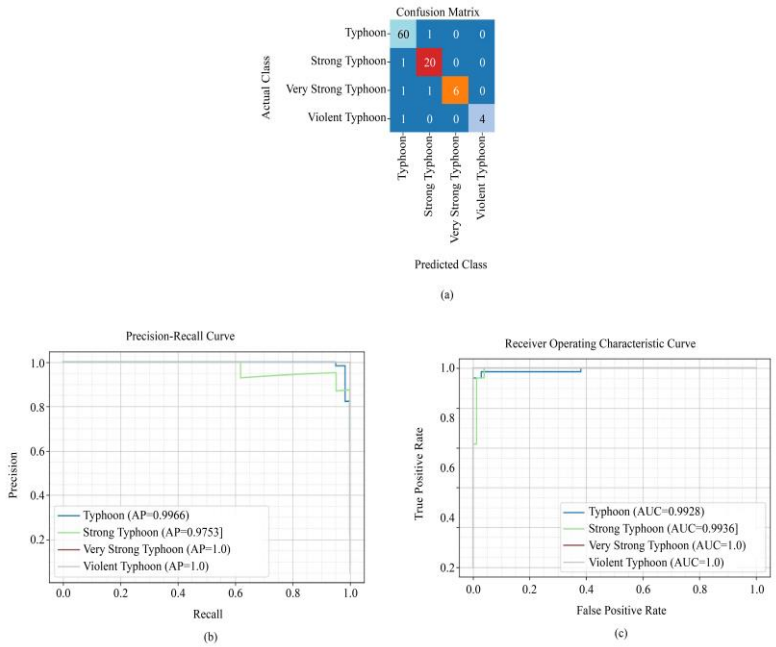

Fig. 7 Training Set (a) Confusion Matrix (b-c) PR and ROC Curve

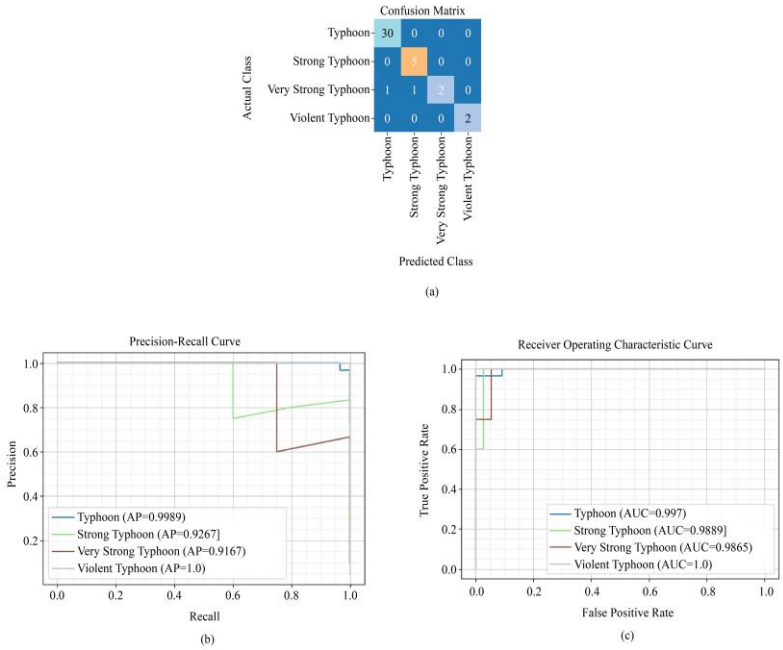

Fig. 8 Testing Set (a) Confusion Matrix (b-c) PR and ROC Curve

The performance of the TCIPCC-IDBODL method on the testing set is illustrated in Figure 8. The confusion matrix illustrated by the TCIPCC-IDBODL method is depicted in Figure 8a. The figure inferred that the TCIPCC-IDBODL approach has accurately detected and categorized above four classes. Likewise, the PR investigation of the TCIPCC-IDBODL approach is shown in Figure 8b. The experimental value described that the TCIPCC-IDBODL approach has gained high PR performance in each class. Lastly, the ROC investigation of the TCIPCC-IDBODL approach is depicted in Figure 8c. The results showed that the TCIPCC-IDBODL approach demonstrated promising outputs with higher ROC values on diverse classes. Table 1 and Figure 9 depict the comprehensive TC grading outputs of the TCIPCC-IDBODL

method. The outputs indicate that the TCIPCC-IDBODL method gains efficient classifier outputs on TRP and TSP.

On TRP, the TCIPCC-IDBODL technique attains $an\ accu_y$ of 94.74%, $prec_n$ of 96.54%, $reca_l$ of 87.15%, $spec_y$ of 97.12%, $F1_{score}$ of 88.17%, and MCC of 89.10%. Also, on TSP, the TCIPCC-IDBODL technique obtains an $accu_y$ of 95.12%, $prec_n$ of 95.03%, $reca_l$ of 87.50%, $spec_y$ of 97.03%, $F1_{score}$ of 88.98%, and MCC of 88.17%.

Table 1. TC grading output of TCIPCC-IDBODL approach under diverse measures

Metrics	TRP	TSP
Accuracy	94.74	95.12
Precision	96.54	95.03
Recall	87.15	87.50
Specificity	97.12	97.03
F1-Score	91.10	88.98
MCC	89.10	88.17

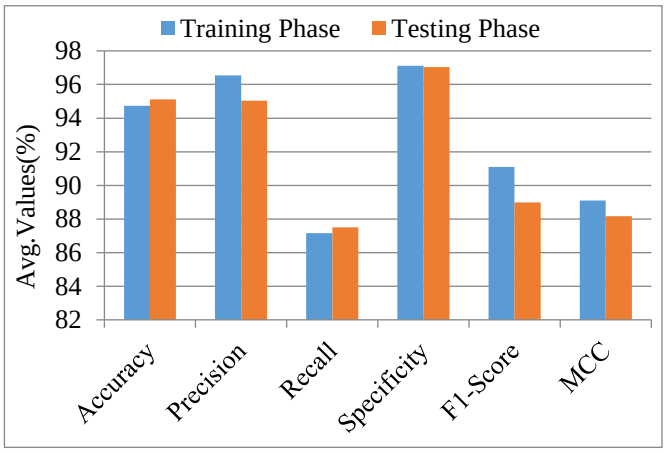

Fig. 9 Average of TCIPCC-IDBODL technique under various measures

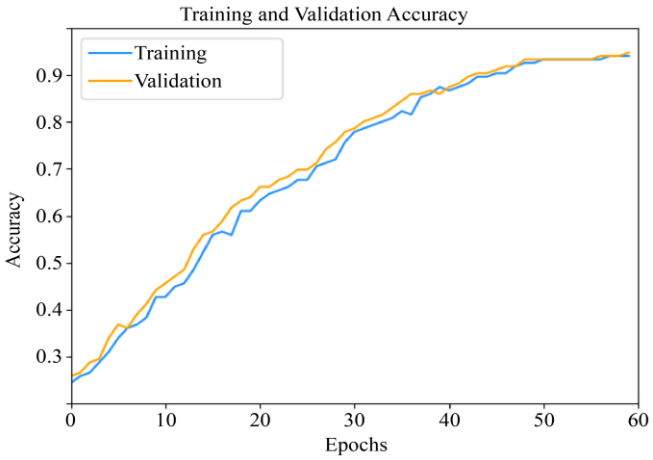

Fig. 10 $Accu_y$ the curve of the TCIPCC-IDBODL technique

The performance of the TCIPCC-IDBODL model is depicted in Figure 10 under training accuracy (TRAAC) and validation accuracy (VALAC) curves. The figure illustrates the performance of the TCIPCC-IDBODL model over multiple epochs, showing continuous improvement in TRAAC and VALAC. This reflects the model's adaptability during pattern detection on TR and TS datasets. The rising VALAC trend emphasizes the capacity of the model to adapt to TR data and effectively classify unseen data, underscoring robust generalization.

Figure 11 demonstrates the training loss (TRLA) and validation loss (VALL) of the TCIPCC-IDBODL model over several epochs. The lessening in TRLA shows the TCIPCC-IDBODL model optimizing the weights and lessening the classifier error on the TR and TS data. The figure associates the TCIPCC-IDBODL method with the TR data, emphasizing its superiority in comprehending patterns in both datasets. Notably, the TCIPCC-IDBODL method steadily enhances its parameters, lessening the discrepancy between the prediction and accurate TR classes.

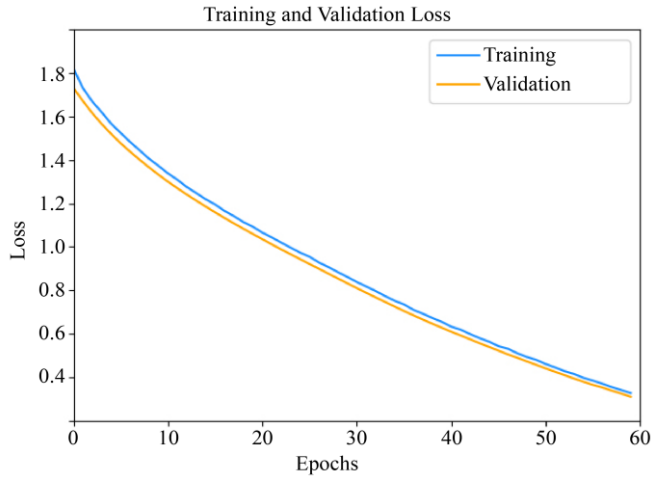

Fig. 11 Loss curve of the TCIPCC-IDBODL technique

Finally, the TCIPCC-IDBODL technique's performance is related to existing techniques in Table 2 and Figure 12 [35-37]. The analysis underlined that the RCTCP model has shown poor accomplishment with the lowest TC grading results. The LEGEMP, ConvLSTM, DCNN, and VGG-16 models have reported slightly boosted TC grading outcomes. Meanwhile, the CNN model has managed to accomplish reasonable performance with $accu_y$ of 92.15%, $prec_n$ of 90.23%, $reca_l$ of 85.10%, and $F1_{score}$ of 83.90%. Nevertheless, the TCIPCC-IDBODL technique demonstrates promising results with $accu_y$ of 95.12%, $prec_n$ of 95.03%, $reca_l$ of 87.50%, and $F1_{score}$ of 88.17%. Therefore, the TCIPCC-IDBODL technique is used to grade TCs accurately.

Table 2. Comparative evaluation of the TCIPCC-IDBODL method with other existing techniques [35-37]

Models	$Accu_y$	$Prec_n$	$Reca_l$	$F1_{Score}$
LEGEMP	82.85	81.71	80.57	79.43
ConvLSTM	72.85	71.64	70.43	69.22

RCTCP	64.28	63.41	62.54	61.67
DCNN	83.40	87.50	86.10	87.00
VGG-16	78.00	94.00	76.00	81.00

CNN	92.15	90.23	85.10	83.90
TCIPCC-IDBODL	95.12	95.03	87.50	88.17

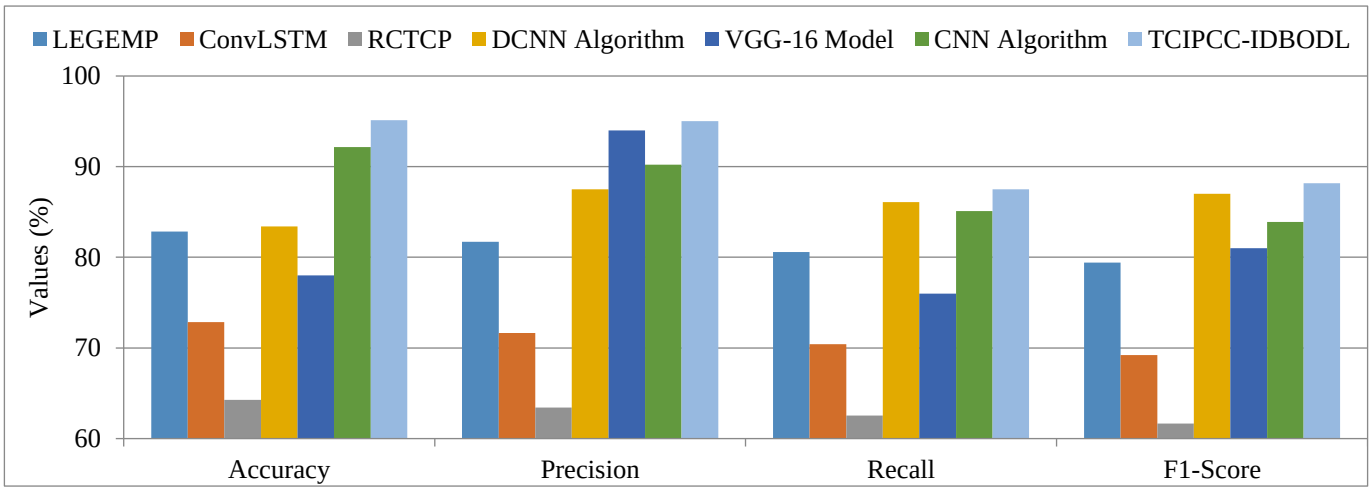

Fig. 12 Comparative analysis of TCIPCC-IDBODL technique with other existing approaches

5. Conclusion

In this manuscript, a novel TCIPCC-IDBODL technique is introduced. The TCIPCC-IDBODL technique aims to predict the TC intensity and classify TC into various types. The TCIPCC-IDBODL technique follows a series of operations to estimate TC intensity and classify TC types, such as pre-processing, feature extraction, and classification. Initially, the TCIPCC-IDBODL technique pre-processes the input images via WF-based noise elimination and DHE-based contrast enhancement. In the TCIPCC-IDBODL method, the SE-EfficientNet model is applied to derive feature vectors from the pre-processed images. Moreover, the SSAE model is used for the prediction and classification purposes. Furthermore, the hyperparameter tuning of the SSAE network is accomplished by using the IDBO technique. A range of investigations was involved in portraying the more significant achievement of the TCIPCC-IDBODL method. The performance validation of the TCIPCC-IDBODL method portrayed a superior accuracy value of 95.12% over existing models. The TCIPCC-IDBODL method's limitations include reliance on a fixed dataset that may not completely capture the diversity of real-world TC scenarios, potentially limiting the model's generalization capability. Furthermore, the computational cost of the proposed methods may affect real-time implementation. Future work should integrate more diverse datasets, optimize computational efficiency, and explore transfer learning techniques to improve model performance in diverse geographical regions. Enhancing model adaptability to diverse environmental conditions could also be a promising avenue for further research.

References

[1] Sarah M. Griffin, Anthony Wimmers, and Christopher S. Velden, "Predicting Short-Term Intensity Change in Tropical Cyclones Using a Convolutional Neural Network," *Weather and Forecasting*, vol. 39, no. 1, pp. 177-202, 2024. [CrossRef] [Google Scholar] [Publisher Link]

[2] Fan Meng et al., "Tropical Cyclone Intensity Probabilistic Forecasting System Based on Deep Learning," *International Journal of Intelligent Systems*, vol. 2023, pp. 1-17, 2023. [CrossRef] [Google Scholar] [Publisher Link]

[3] Lujin Li et al., "Classification of Tropical Cyclone Intensity Based on Deep Learning and YOLO V5," *Conference on Advances in Artificial Intelligence and Security*, pp. 280-291, 2022. [CrossRef] [Google Scholar] [Publisher Link]

[4] S.L. Gan et al., "Short-Term Prediction of Tropical Cyclone Track and Intensity via Four Mainstream Deep Learning Techniques," *Journal of Wind Engineering and Industrial Aerodynamics*, vol. 244, 2024. [CrossRef] [Google Scholar] [Publisher Link]

[5] Buo-Fu Chen, Yu-Te Kuo, and Treng-Shi Huang, "A Deep Learning Ensemble Approach for Predicting Tropical Cyclone Rapid Intensification," *Atmospheric Science Letters*, vol. 24, no. 5, pp. 1-11, 2023. [CrossRef] [Google Scholar] [Publisher Link]

[6] Hyeyoon Jung et al., "Tropical Cyclone Intensity Estimation through Convolutional Neural Network Transfer Learning Using Two Geostationary Satellite Datasets," *Frontiers in Earth Science*, vol. 11, pp. 1-15, 2023. [CrossRef] [Google Scholar] [Publisher Link]

[7] Wenke Wang, and Xin Wang, "The Prediction Method of Tropical Cyclone Intensity Change Based on Deep Learning," *ESS Open Archive*, pp. 1-12, 2020. [CrossRef] [Google Scholar] [Publisher Link]

[8] Liang Wang et al., "Forecasting Tropical Cyclone Tracks in the Northwestern Pacific Based on A Deep-Learning Model," *Geoscientific*

Model Development, vol. 16, no. 8, pp. 2167-2179, 2023. [CrossRef] [Google Scholar] [Publisher Link]

[9] Dasol Kim, and Corene J. Matyas, "Classification of Tropical Cyclone Rain Patterns Using Convolutional Auto Encoder," *Scientific Reports*, vol. 14, no. 1, 2024. [CrossRef] [Google Scholar] [Publisher Link]

[10] Arpit Kapoor et al., "Cyclone Trajectory and Intensity Prediction with Uncertainty Quantification Using Variational Recurrent Neural Networks," *Environmental Modelling & Software*, vol. 162, pp. 1-13, 2023. [CrossRef] [Google Scholar] [Publisher Link]

[11] Wei Tian et al., "Short-Term Intensity Prediction of Tropical Cyclones Based on Multi-Source Data Fusion with Adaptive Weight Learning," *Remote Sensing*, vol. 16, no. 6, pp. 1-21, 2024. [CrossRef] [Google Scholar] [Publisher Link]

[12] Jinkai Tan et al., "Tropical Cyclone Intensity Estimation Using Himawari-8 Satellite Cloud Products and Deep Learning," *Remote Sensing*, vol. 14, no. 4, pp. 1-18, 2022. [CrossRef] [Google Scholar] [Publisher Link]

[13] Wei Tian et al., "Estimating Tropical Cyclone Intensity Using Dynamic Balance Convolutional Neural Network from Satellite Imagery," *Journal of Applied Remote Sensing*, vol. 17, no. 2, 2023. [CrossRef] [Google Scholar] [Publisher Link]

[14] Wei Tian et al., "Predicting the Intensity of Tropical Cyclones over the Western North Pacific Using Dual-Branch Spatio-Temporal Attention Convolutional Network," *Weather and Forecasting*, vol. 39, no. 5, pp. 807-819, 2024. [CrossRef] [Google Scholar] [Publisher Link]

[15] Jianbo Xu et al., "Tropical Cyclone Size Estimation Based on Deep Learning Using Infrared and Microwave Satellite Data," *Frontiers in Marine Science*, vol. 9, 2022. [CrossRef] [Google Scholar] [Publisher Link]

[16] Y. Vahidhabanu et al., "Cyclone Intensity Detection and Classification Using a Attention-Based 3D Deep Learning Model," *Proceedings of Fourth International Conference on Computing, Communications, and Cyber-Security*, pp. 505-516, 2023. [CrossRef] [Google Scholar] [Publisher Link]

[17] Chong Wang, Xiaofeng Li, and Gang Zheng, "Tropical Cyclone Intensity Forecasting Using Model Knowledge Guided Deep Learning Model," *Environmental Research Letters*, vol. 19, no. 2, pp. 1-10, 2024. [CrossRef] [Google Scholar] [Publisher Link]

[18] Chuan-Hui Zhang, and Chang-Jiang Zhang, "Rapid Intensification Forecast for Tropical Cyclone by Combining Multi-ConvLSTM Model with Infrared and Microwave Satellite Images," *Conference on Infrared, Millimeter, Terahertz Waves and Applications*, vol. 12565, pp. 240-245, 2023. [CrossRef] [Google Scholar] [Publisher Link]

[19] Chang-Jiang Zhang et al., "Deep Learning and Wavelet Transform Combined with Multi-channel Satellite Images for Tropical Cyclone Intensity Estimation," *IEEE Journal of Selected Topics in Applied Earth Observations and Remote Sensing*, vol. 18, pp. 4711-4735, 2025. [CrossRef] [Google Scholar] [Publisher Link]

[20] Wen Yang et al., "Enhancing Tropical Cyclone Intensity Estimation from Satellite Imagery through Deep Learning Techniques," *Journal of Meteorological Research*, vol. 38, no. 4, pp. 652-663, 2024. [CrossRef] [Google Scholar] [Publisher Link]

[21] Biao Tong B. et al., "Deep Learning Based Simulation of Tropical Cyclone Genesis in Northwest Pacific," *Journal of Wind Engineering and Industrial Aerodynamics*, vol. 257, 2025. [CrossRef] [Google Scholar] [Publisher Link]

[22] Jeong Hwan Kim et al., "Improvement in Forecasting Short-Term Tropical Cyclone Intensity Change and Their Rapid Intensification Using Deep Learning," *Artificial Intelligence for the Earth Systems*, vol. 3, no. 2, pp. 1-16, 2024. [CrossRef] [Google Scholar] [Publisher Link]

[23] Tianyi Lv et al., "Research on Typhoon Prediction by Integrating Numerical Simulation and Deep Learning Methods," *Atmosphere*, vol. 16, no. 1, pp. 1-17, 2025. [CrossRef] [Google Scholar] [Publisher Link]

[24] D. Yella Krishna et al., "Cyclone Intensity Estimation Using Deep Learning," *Journal of Electrical Systems*, vol. 20, no. 6s, pp. 2706-2715, 2024. [CrossRef] [Publisher Link]

[25] Xinyu Wang et al., "VQLTI: Long-Term Tropical Cyclone Intensity Forecasting with Physical Constraints," *arXiv*, pp. 1-9, 2025. [CrossRef] [Google Scholar] [Publisher Link]

[26] Manish Kumar Mawatwal, and Saurabh Das, "An End-to-End Deep Learning Framework for Cyclone Intensity Estimation in North Indian Ocean Region Using Satellite Imagery," *Journal of the Indian Society of Remote Sensing*, vol. 52, no. 10, pp. 2165-2175, 2024. [CrossRef] [Google Scholar] [Publisher Link]

[27] Yukun Xiao et al., "Sealing Strip Acoustic Performance Evaluation Using WF-VMD-Based Signal Enhancement Method," *Applied Acoustics*, vol. 217, 2024. [CrossRef] [Google Scholar] [Publisher Link]

[28] Boyina Subrahmanyeswara Rao, "Dynamic Histogram Equalization for Contrast Enhancement for Digital Images," *Applied Soft Computing*, vol. 89, 2020. [CrossRef] [Google Scholar] [Publisher Link]

[29] Umit Atila et al., "Plant Leaf Disease Classification Using Efficient Net Deep Learning Model," *Ecological Informatics*, vol. 61, 2021. [CrossRef] [Google Scholar] [Publisher Link]

[30] Ravi Teja N.V.S. Chappa, and Mohamed El-Sharkawy, "Squeeze-and-Excitation Squeeze Next: An Efficient DNN for Hardware Deployment," *2020 10th Annual Computing and Communication Workshop and Conference (CCWC)*, Las Vegas, NV, USA, pp. 691-697, 2020. [CrossRef] [Google Scholar] [Publisher Link]

[31] Yi He, Yunan Yao, and Hongsen Ou, "Status Recognition of Marine Centrifugal Pumps Based on a Stacked Sparse Auto-Encoder," *Applied Sciences*, vol. 14, no. 4, pp. 1-15, 2024. [CrossRef] [Google Scholar] [Publisher Link]

[32] Zhaodong Guo et al., "Research on Indoor Environment Prediction of Pig House Based on OTDBO–TCN–GRU Algorithm," *Animals*, vol. 14, no. 6, pp. 1-20, 2024. [CrossRef] [Google Scholar] [Publisher Link]

[33] Oluwatayomi Rereloluwa Adegboye et al., "Chaotic Opposition Learning with Mirror Reflection and Worst Individual Disturbance Grey Wolf Optimizer for Continuous Global Numerical Optimization," *Scientific Reports*, vol. 14, no. 1, pp. 1-41, 2024. [CrossRef] [Google Scholar] [Publisher Link]

[34] Kaggle, INSAT3D Infrared & Raw Cyclone Imagery (2012-2021), 2022. [Online]. Availble: https://www.kaggle.com/datasets/sshubam/insat3d-infrared-raw-cyclone-images-20132021

[35] Senthilkumar Jayaraman et al., "Enhancing Cyclone Intensity Prediction for Smart Cities Using a Deep-Learning Approach for Accurate Prediction," *Atmosphere*, vol. 14, no. 10, pp. 1-16, 2023. [CrossRef] [Google Scholar] [Publisher Link]

[36] Biao Tong et al., "Estimation of Tropical Cyclone Intensity via Deep Learning Techniques from Satellite Cloud Images," *Remote Sensing*, vol. 15, no. 17, pp. 1-26, 2023. [CrossRef] [Google Scholar] [Publisher Link]

[37] Franciskus Antonius Alijoyo et al., "Advanced Hybrid CNN-Bi-LSTM Model Augmented with GA and FFO for Enhanced Cyclone Intensity Forecasting," *Alexandria Engineering Journal*, vol. 92, pp. 346-357, 2024. [CrossRef] [Google Scholar] [Publisher Link]